ISSN 1392–1207. MECHANIKA. 2014 Volume 20(6): 535–542

Automotive stabilizer bar – stabilizer bar strength calculations using FEM, ovalization of radial areas of tubular stabilizer bars

A.M. Wittek*, D. Gąska, B. Łazarz***, T. Matyja******
**ThyssenKrupp Federn & Stabilisatoren GmbH, Wienerstr. 35, 58135 Hagen,Germany, E-mail: adam.wittek@t-online.de*
***Silesian University of Technology, Faculty of Transport, Krasińskiego St. 8, 40-019 Katowice, Poland, E-mail: damian.gaska@polsl.pl*
****Silesian University of Technology, Faculty of Transport, Krasińskiego St. 8, 40-019 Katowice, Poland, E-mail: boguslaw.lazarz@polsl.pl*
*****Silesian University of Technology, Faculty of Transport, Krasińskiego St. 8, 40-019 Katowice, Poland, E-mail: tomasz.matyja@polsl.pl*

crossref http://dx.doi.org/10.5755/j01.mech.20.6.7706

1. Introduction

In the simplest application, solid stabilizer bar is substituted by a tubular stabilizer bar where the tube cross-section is constant over the entire stabilizer bar length. The spring rate of a stabilizer bar arises from the overall deformation of the areas under bending and torsional stresses under a given load. A specific cross-section (area moment of inertia) is needed to achieve a required rate. The tube stiffness against buckling and denting limits the reduction of the wall thickness.

Therefore the relation of the outer diameter to the wall thickness should not exceed 6.5 to 7.5 mm. The bent transitions between the back and the arms of a stabilizer bar as a rule constitute the highly stressed areas of this element. Due to the complex geometry (cross–section – elliptic) in these areas occur increased stresses in consequence of which the required durability may not be achieved [1-4].

The analytical calculation software (for example St3d from ThyssenKrupp Federn & Stabilisatoren GmbH) is not designed in such a way as to be able to take the cross–section deformations – changes into consideration. The changes in cross–section (changes in the area moment of inertia) in bent transitions are to be analytically calculated by means of approximation of the cross–sections.

Tubular stabilizer bar (cold and hot) bending is accompanied by many phenomena characteristic for this process which may be divided into two groups:

1) Changes in shape of the tube cross–section [5, 6]:

• Ovalization of the tube cross–section – grows with the increase of the possibility of free deformation of this wall. Additional internal stresses which occur during bending, being the effect of strain hardening, may contribute to the occurrence of microcracks and corrosion at the grain boundaries.

• Change in the tube wall thickness – during the tube bending process the wall thickness changes in the entire bending area. Since the stabilizer bar radial areas have to meet various strength and structural requirements and criteria, the initial tube thickness is to be selected in such a way so as to meet these requirements. In practice, it turns out that wall thinning during stabilizer bar cold bending rarely influences the strength of the radial area in view of a simultaneous work hardening of the pipe material. Wall thinning is of great importance if the stabilizer bar is put to further heat treatment, e.g. tempering or normalizing, or if it will operate in a corrosion environment [4- 6].

• Elastic recovery deformation – apart from the plastic deformation, certain elastic deformations always occur during metal deformation. Also in the tubular stabilizer bar bending area, apart from durable plastic deformations occur elastic deformations which after the cessation of action of deforming stresses reduce the overall deformation, tending to restore the original shape of the tube. This phenomenon is called tube spring–back and has to be taken into consideration when designing the tools so that the finished stabilizer bar complies with the required accuracy [5, 6-8].

• Neutral layer shift – the neutral layer is a curvilinear surface separating material layers subject to deformations with different characters. It shifts during bending in the direction of the centre of curvature – a change in the wall thickness and a deformation of the cross–section cause a permanent change in the moment of inertia and the position of the centre of gravity of the cross–section of bent tube, with simultaneous deformation hardening of the material. The neutral layer shift is influenced by the level of longitudinal stresses during bending. In case of bending combined with stretching the neutral layer moves in the direction of the centre of curvature, and in case of bending with compression – moves more away of it [5, 6, 9].

2) Changes in strength properties – cold bending of tubular stabilizer bars is accompanied by many phenomena which limit the possibility of further plastic deformation. These factors include: material's loss of ability to plastic deformation, increase of the yield point, decrease of impact strength and the like. An additional portion of stored (hidden) energy supplied to stretched outer layers of the bent tube material may activate and intensify certain internal physicochemical processes, including also destructive, such as creeping processes. In order to partially prevent these phenomena, hot bending of tubular stabilizer bars is recommended. During hot bending of steel tubes at the temperature between 850 – 930°C the deformation hardening no longer occurs [5, 6, 10].

2. Materials and methods

2.1 Approximation of cross–sections

If we regard the above cross–sections as geometric objects, they are very difficult to manage mathematically. Therefore it is necessary to configure them computably by means of an approximation through „simpler“ functions, based on measured values [3, 4, 11-13].

Initial value (cross–section–circular) (Fig. 1): outside-diameter D_a, mm; wall thickness w, mm.

Measured value (cross–section–elliptical) (Fig. 1): the outer width corresponds to the width of the bending tool; maximum width, outer D_w, mm; the internal width, at the same point as the maximum outside width c, mm; maximum height, outside e, mm; wall thickness below g_2, mm; wall thickness above g_3, mm.

On the basis of these two values, the wall thickness at the relevant point may be determined:

$$g_1 = \frac{D_w - c}{2}, \text{ mm} \tag{1}$$

(assumed to be equal on both sides)

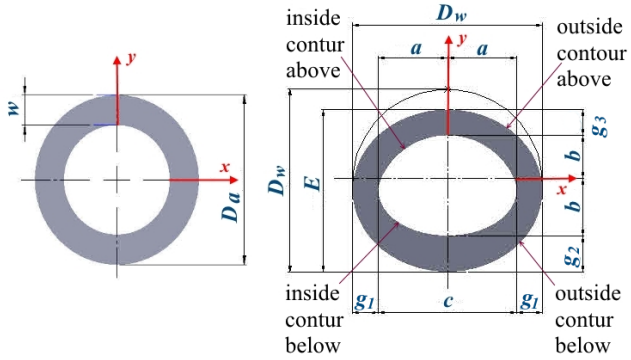

Fig. 1 Cross–section of the tubular stabilizer bar in the main radial zone – main geometric parameters

As point of origin, the point in the cross–section is determined which lies in the width in the middle of the cross-section and in the height at the distance of $a/2$ from the lower edge. Thus the x–axis lies in the axis of the greater width, the y–axis points upwards. The bottom half of the outer contour is assumed to be circular with the diameter D_w because it is hindered by the tool at a warp [3, 4, 11-13]. The internal contour of the bottom half as well as both contours of the upper half should be described by ellipses:

$$\frac{x^2}{a^2} + \frac{y^2}{b^2} = 1 \tag{2}$$

Consequently, to determine the ellipses both half–axes a and b, respectively, have to be found. To both ellipses of the internal contour must apply:

$$a = \frac{D_w}{2} - g_1 \tag{3}$$

and to the upper outer contour:

$$a = b = \frac{D_w}{2} \tag{4}$$

The y–half–axes are thus:

- inside, below (Fig. 1):

$$b = \frac{D_w}{2} - g_2; \tag{5}$$

- outside, above (Fig. 1):

$$b = E - \frac{D_w}{2}; \tag{6}$$

- inside, above (Fig. 1):

$$b = E - \frac{D_w}{2} - g_3. \tag{7}$$

Since the approach $I_p = I_x + I_y$ is actually correct for circular cross–sections only, the integral:

$$I_p = \int r^2 dF = \int \left(x^2 + y^2\right) dF = I_x + I_y \tag{8}$$

has always to be solved. Since it is impossible in case of the present cross–section due to irregular boundaries, the sums of the axial area moments of inertia may be used for the rough estimate.
where:

$$I_x = \int y^2 dF = \int y^2 \, x dy, \tag{9}$$

$$I_y = \int x^2 dF = \int x^2 \, y dx, \tag{10}$$

$$I_{x1} = \int_{\left(-\frac{D_w}{2}\right)}^{-\left(\frac{D_w}{2} - g_2\right)} (y)^2 \sqrt{\left(\frac{D_w}{2}\right)^2 - (y)^2}\, dy, \tag{11}$$

$$I_{x2} = \int_{-\left(\frac{D_w}{2} - g_2\right)}^{0} (y)^2 \left[\sqrt{\left(\frac{D_w}{2}\right)^2 - (y)^2} - \left(\frac{D_w}{2} - g_1\right) \sqrt{1 - \frac{(y)^2}{\left(\frac{D_w}{2} - g_2\right)^2}} \right] dy, \tag{12}$$

$$I_{x3} = \int_{0}^{E-g_3-\frac{D_w}{2}} (y)^2 \left[\left(\frac{D_w}{2}\right) \sqrt{1-\frac{(y)^2}{\left(E-\frac{D_w}{2}\right)^2}} - \left(\frac{D_w}{2}-g_1\right) \sqrt{1-\frac{(y)^2}{\left(E-\frac{D_w}{2}-g_3\right)^2}} \right] dy\,, \tag{13}$$

$$I_{x4} = \int_{E-g_3-\frac{D_w}{2}}^{E-\frac{D_w}{2}} (y)^2 \left[\left(\frac{D_w}{2}\right) \sqrt{1-\frac{(y)^2}{\left(E-\frac{D_w}{2}\right)^2}} \right] dy\,, \tag{14}$$

$$I_{y1,u} = \int_{-\frac{D_w}{2}}^{-\left(\frac{D_w}{2}-g_2\right)} x^2 \sqrt{\left(\frac{D_w}{2}\right)^2 - x^2}\, dx\,, \tag{15}$$

$$I_{y1,o} = \int_{-\frac{D_w}{2}}^{-\left(\frac{D_w}{2}-g_2\right)} x^2 \left[\left(E-\frac{D_w}{2}\right) \sqrt{1-\frac{x^2}{\left(\frac{D_w}{2}\right)^2}} \right] dx\,, \tag{16}$$

$$I_{y2,u} = \int_{-\left(\frac{D_w}{2}-g_2\right)}^{0} x^2 \left[\sqrt{\left(\frac{D_w}{2}\right)^2 - x^2} - \left(\frac{D_w}{2}-g_2\right) \sqrt{1-\frac{x^2}{\left(\frac{D_w}{2}-g_1\right)^2}} \right] dx\,, \tag{17}$$

$$I_{y2,o} = \int_{-\left(\frac{D_w}{2}-g_2\right)}^{0} x^2 \left[\left(E-\frac{D_w}{2}\right) \sqrt{1-\frac{x^2}{\left(\frac{D_w}{2}\right)^2}} - \left(E-\frac{D_w}{2}-g_3\right) \sqrt{1-\frac{x^2}{\left(\frac{D_w}{2}-g_1\right)^2}} \right] dx\,. \tag{18}$$

Since the moment of inertia is not based on the center, it must be corrected for the Steiner's shift share:

$$I_x = 2\left(I_{x1} + I_{x2} + I_{x3} + I_{x4}\right) - y_s{}^2\, Q_s\,, \tag{19}$$

where $y_s{}^2 \cdot Q_s$ is Steiner's shift share, Q_s is cross section (deformed) of the bent tube (with application of approximation functions), y_s is– displacement of the center of gravity in the y –axis:

$$I_y = 2\left(I_{y1,u} + I_{y1,o} + I_{y2,u} + I_{y2,o}\right). \tag{20}$$

A correction by the set of Steiner is not necessary here, since the centroid lies in the $x-$ direction at zero. Alternatively, it is also possible to determine the polar area moment of inertia by combining the „bottom“ semicircle and the „upper“ ellipse and afterwards subtracting the inner ellipses. The total area moment of inertia combined according to the elementary formula is then:

$$I_{p,e} = I_{c,bo} + I_{e,ao} - I_{e,ab} - I_{e,ai}\,. \tag{21}$$

In the individual case the following proportions are concerned [3, 4, 11-13]:

1. Half circle “below”, outside (Fig. 1):

$$I_{c,bo} = \frac{\pi}{4}\left(\frac{D_w}{2}\right)^4; \tag{22}$$

2. Half ellipse “above”, outside (Fig. 1):

$$I_{e,oa} = \frac{\pi}{2} \frac{\left(\frac{D_w}{2}\right)^3 \left(E-\frac{D_w}{2}\right)^3}{\left(\frac{D_w}{2}\right)^2 + \left(E-\frac{D_w}{2}\right)^2}; \tag{23}$$

3. Half ellipse “above”, below (Fg. 1):

$$I_{e,ab} = \frac{\pi}{2} \frac{\left(\frac{D_w}{2}-g_2\right)^3 \left(\frac{D_w}{2}-g_1\right)^3}{\left(\frac{D_w}{2}-g_2\right)^2 + \left(\frac{D_w}{2}-g_1\right)^2}; \tag{24}$$

4. Half ellipse “above”, inside (Fig. 1):

$$I_{e,ai} = \frac{\pi}{2} \frac{\left(E-\frac{D_w}{2}-g_3\right)^3 \left(\frac{D_w}{2}-g_1\right)^3}{\left(E-\frac{D_w}{2}-g_3\right)^2 + \left(\frac{D_w}{2}-g_1\right)^2}. \tag{25}$$

The section moduli are defined as:

$$W_x = \frac{2I_x}{h},\; W_y = \frac{2I_y}{h},\; W_p = \frac{2I_p}{h} = \frac{2\left(I_x + I_y\right)}{h}, \tag{26}$$

where h is the diameter of the cross-section. Here, it should be considered that depending on the direction of viewing for h due to different diameters a different value arises:

$$W_{p,E} = 2\,\frac{I_{p,E}}{h}\,. \tag{27}$$

For W_x the diameter is E, for W_y it is D_w, thus the axial section moduli are:

$$W_x = \frac{2I_x}{E}\,,\; W_y = \frac{2I_y}{D_w}\,, \tag{28}$$

applies to the straight pipe:

$$W_{g,x} = W_{g,y}\,\frac{2I_{x,g}}{D_a}\,. \tag{29}$$

The theoretical bending stresses at a bent, deformed tube change compared to the theoretical bending stresses at a straight, undeformed tube by the following factors [3, 4, 11-13]:

- Bending stress ratio at the y –axis:

$$\xi_{\sigma,y} = \frac{W_{g,x}}{W_x} = 1.12\,; \tag{30}$$

- Bending stress ratio at the x –axis:

$$\xi_{\sigma,x} = \frac{W_{g,y}}{W_y} = 1.04\,. \tag{31}$$

The values which have been calculated according to the abovementioned formulas to a great extent correspond to the bending tests (actual deformation during cold bending) (Figs. 1 and 2).

2.1 Measurements of geometric parameters

The geometry analysis included two stabilizer bars which are now widely used in industry (MQB and Suzuki). Stabilizers geometry of ovalization was measured in points shown in Fig. 2 (cold – formed MQB stabilizer).

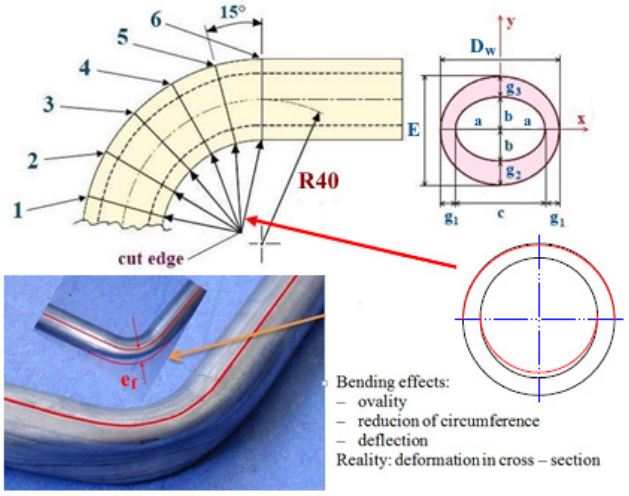

Fig. 2 Measurement of geometrical changes (ovality, wall thickness) in cold bent tubular stabilizer bar $R_{p0.2}$ – 0.2% yield strength

$$e_f = \frac{k_f - R_{p0.2}}{p_0}\,sin\frac{\alpha}{2}\,s_0\,sin\varphi\,, \tag{32}$$

$$\varepsilon = \frac{D_0 - e_f}{2R_{th}}\,, \tag{33}$$

where R_{th} is theoretical bending radius, D_0 is outer diameter of tubular stabilizer bar, e_f is deformation of tubular stabilizer bar, α is bending angle, φ is apex angle, k_f is flow stress, p_0 is compressive stress, s_0 is output wall thickness.

Results in the form of the characteristics of the geometric parameters are shown in Fig. 3 (MQB tubular stabilizer bar). It can be clearly seen that the diameter and wall thicknesses vary considerably in subsequent measuring points. On the basis of the geometry measurements the CAD models, shown in Fig. 4, were made.

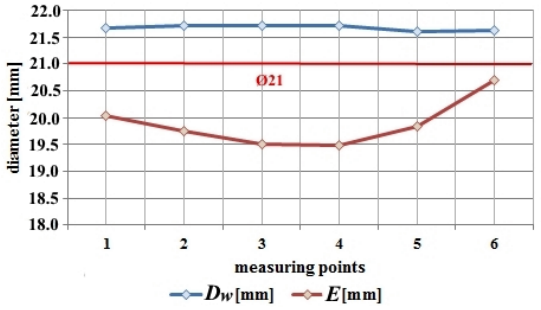

a

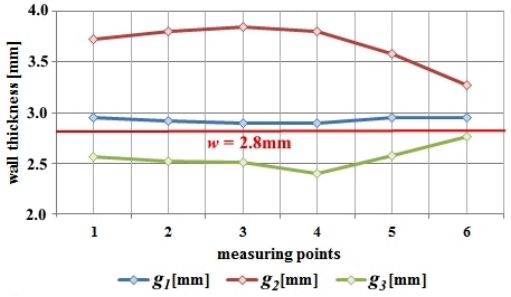

b

Fig. 3 Results of geometrical changes – ovality: a) wall thickness, b) in cold bent tubular stabilizer bar (MQB)

A change in cross–section for the FEM calculation models and their course along the neutral axis has been shown in Figs. 4, a and b.

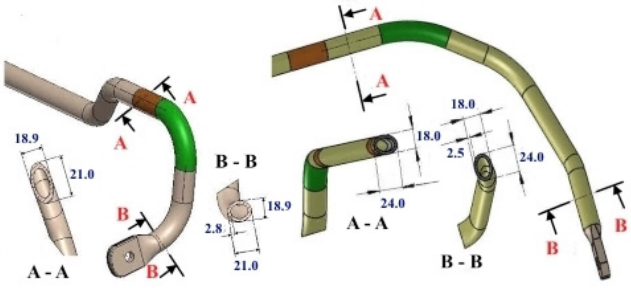

a b

Fig. 4 Critical cross–sections of tubular stabilizer bars (CAD model): a) MQB, b) Suzuki

3. Results and discussion

FEM models were built based on previous measurements using the necessary simplifications in the geometry. Stabilizer bars were loaded by displacement given at the point of attachment to the moving parts of the vehicle suspension. The supports at bearings were modeled as MPC elements. Strength analysis was made using HyperWorks and Abaqus systems, and fatigue analysis using nCode DesignLife system [14-16] – calculation and design parameters (see the Table 1, 2 – item 4-10, Figs. 4 and 12).

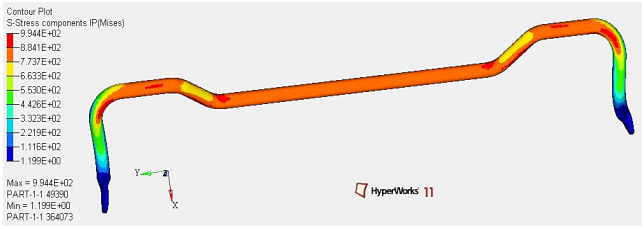

Fig. 5 Stress distribution in the loaded tubular stabilizer bar (MQB) with circular cross–section

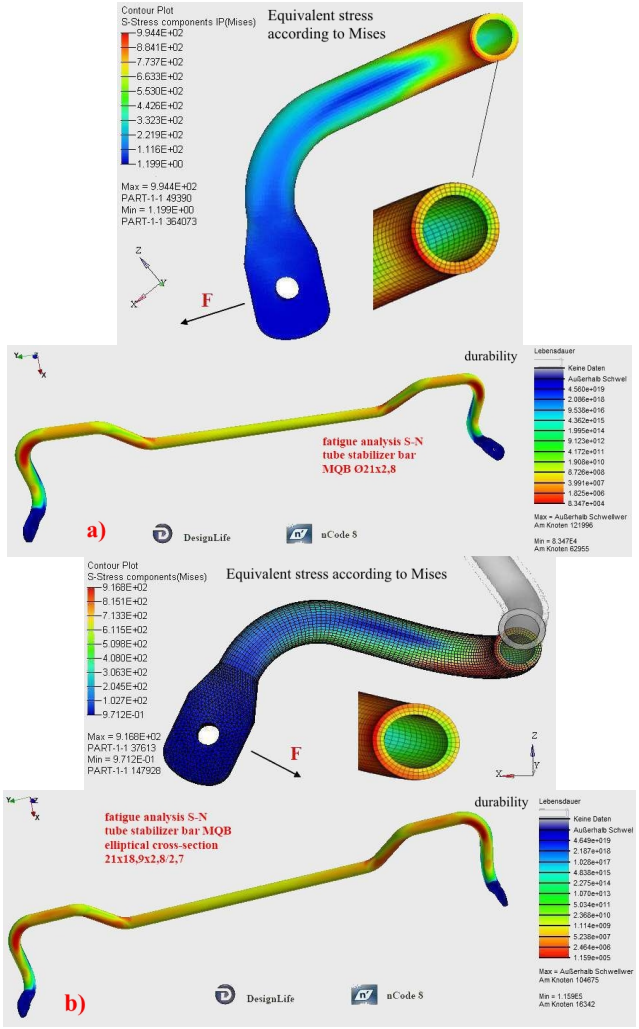

Fig. 6 Stress distribution and fatigue strength / durability of tubular stabilizer bar (MQB) with circular and elliptical cross–section: a) circular cross–section (perfect cross–section const.), b) elliptical cross–section

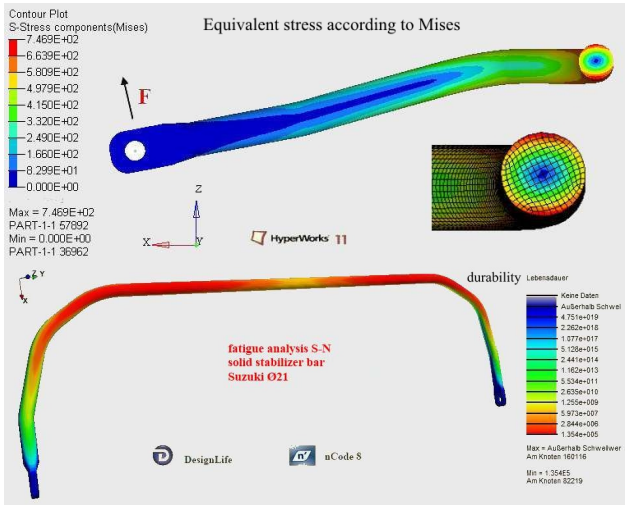

Fig. 7 Distribution of stress and fatigue strength (maximum number of fatigue cycles) of solid stabilizer bars (Suzuki) with circular cross–section

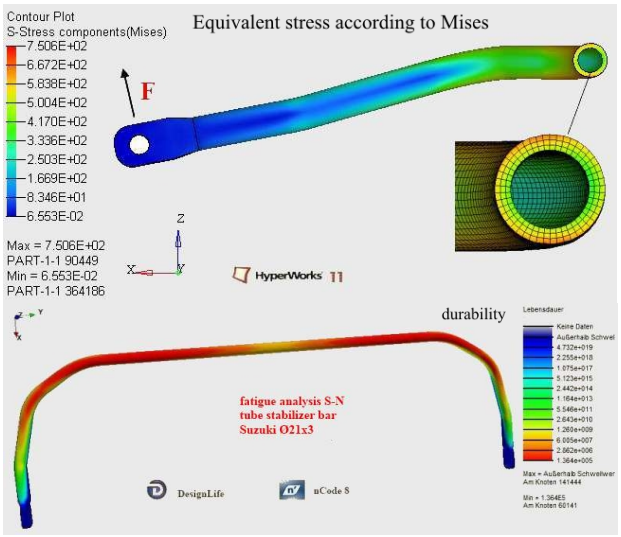

Fig. 8 Distribution of stress and fatigue strength (maximum number of fatigue cycles) of tubular stabilizer bars (Suzuki) with circular cross–section

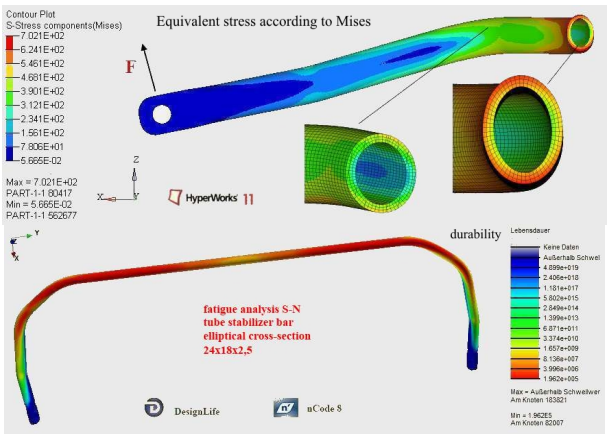

Fig. 9 Distribution of stress and fatigue strength (maximum number of fatigue cycles) of tubular stabilizer bars (Suzuki) with elliptical cross–section (elliptical cross–section – tubular stabilizer bar, ovalisation in the major radial areas)

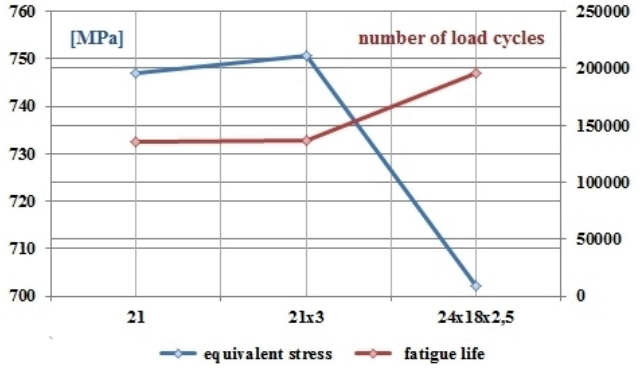

a

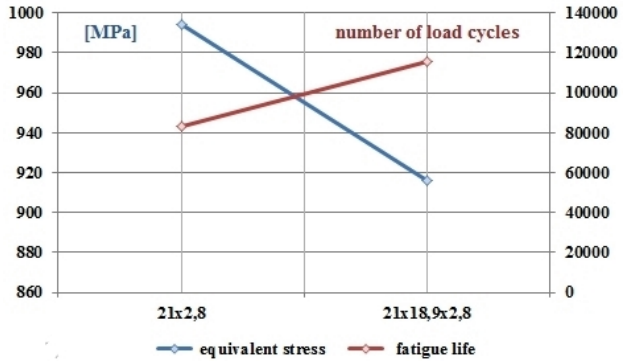

b

Fig. 10 Fatigue strength / durability of MQB tubular stabilizer bar: a) number of fatigue cycles (Figs. 7, 8, 9), b) number of fatigue cycles (Fig. 6)

The Figs. 5- 9 show the results of the FEM calculations – the equivalent stress levels and the endurance strength values for the selected stabilizer bars. As can be seen (Figs. 10, a and b), the number of load changes for stabilizer bars increases with the oval – elliptic cross–section in bent areas (cross–section is oval – elliptic, but constant and runs along the neutral line (Figs. 6 and 9). The section modulus in the load axis increased due to the oval cross–section (Table 2). Consequence – the equivalent stresses decrease. In fact, the cross–sections are not constant in the bent areas – changes in cross–section correspond to a greater extent to the cross–section geometry shown in Figs. 1 and 2. The FEM calculations (Figs. 5-9, Tables 1 and 2) show that the changes in stabilizer bar cross–section in bent areas lead to the stress reduction or a minimum stress increase. The real changes in cross–section (Figs. 1 and 2) are very difficult to model using the 3D CAD systems. Therefore the simplifications have to be provided which with small deviations correspond to the reality. For analytic calculations in the threatened, most strained cross–sections the use of the approximation method described in sub–item 2.1 is recommended.

Changes in cross–section in the FEM calculation models (Figs. 6-9) and their course along the neutral axis has been shown in Figs 4, a and b.

The fatigue strength in the form of number of cycles to destroy, shown in Figs. 6-9, for all subjects exhibit similar values instead of geometry shape of stabilizer bar. However, it should be noted that the stabilizer bar with the ovalization (both the MQB and Suzuki) has the highest fatigue strength. The results and respective geometric parameters of the stabilizer bars are shown in Tables 1 and 2 (item 11-12, Figs. 6, b; 9 and 10).

Table 1

The results and respective geometric parameters of the MQB stabilizer bar

Section properties of MQB		Tube Ø21x2.8	Oval 21x18.9x2.8
1	Area, mm^2	160.1	151.83
		100.00%	94.83%
2	Polar moment of inertia of the surface at the center of gravity, mm^4	I_p = 13571.3	I_p =11393.26
		I_x = 6785.65	I_x = 5180.59
		I_y = 6785,65	I_y = 6212,67
		100.00%	83.95%
3	Gravity center – ralative to origin of part, mm	X = 2667.8	X = 2667.8
		Y = – 403.5	Y = – 403.5
		Z = –10	Z = –10
4	Spring rate of the stabilizer bar, N/mm (Fig. 12)	57.52	48.25
		100.00%	83.90%
5	Deformation of stabilizer bar 2s, mm (Fig. 12)	40	40
6	Bending radii R, mm	40	40
7	Distance between the bearings l, mm (Fig. 12)	697.5	697.5
8	Span of arm L, mm (Fig. 12)	797.5	797.5
9	Material	55Cr3	34MnB5
10	R_m, MPa	1400 – 1700	1700
Results			
11	Equivalent stress acc. to Mises (FEM), MPa	994 (Fig. 6, a)	916 (Fig. 6, b)
		100%	92.15%
12	Fatigue strength / durability, number of fatigue cycles	$8.347e^4$ (Fig. 6, a)	$1.159e^5$ (Fig. 6, b)

Table 2

The results and respective geometric parameters of the Suzuki stabilizer bar

Section properties of Suzuki		Solid Ø21	Tube Ø21x3	Oval 24x18x2.5
1	Area, mm^2	346.36	169.65	146.16
		100%	48.98%	42.19%
2	Polar moment of inertia of the surface at the center of gravity, mm^4	I_p = 19093.12	I_p = 14123.02	I_p = 12713.12
		I_x = 9546.56	I_x = 7061,51	I_x = 4831.51
		I_y = 9546.56	I_y =7061,51	I_y = 7881.61
		100%	73.96%	66.58%
3	Gravity center – ralative to origin of part, mm	X = 280.00	X = 280.00	X = 280.00
		Y = 484.96	Y = 484.96	Y = 484.96
		Z = 0.00	Z = 0.00	Z = 0.00
4	Spring rate, N/mm (Fig. 12)	17.16	12.69	11.45
		100%	73.95%	66.50%
5	Deformation of stabilizer bar 2s, mm (Fig. 12)	117	117	117
6	Bending radii R, mm	50, 83, 115	50, 83, 115	50, 83, 115
7	Distance between the bearings l, mm	499.5	499.5	499.5
8	Span of arm L, mm (Fig. 12)	961.5	961.5	961.5
9	Material	55Cr3	34MnB5	34MnB5
10	R_m MPa	1400 – 1700	1700	1700
Results				
11	Equivalent stress acc. to Mises (FEM), MPa	746 (Fig. 7)	750 (Fig. 8)	702 (Fig. 9)
		100%	100.53%	94.00%
12	Fatigue strength / durability, [number of fatigue cycles	1.354e5 (Fig. 7)	1.364e5 (Fig. 8)	1.962e5 (Fig. 9)

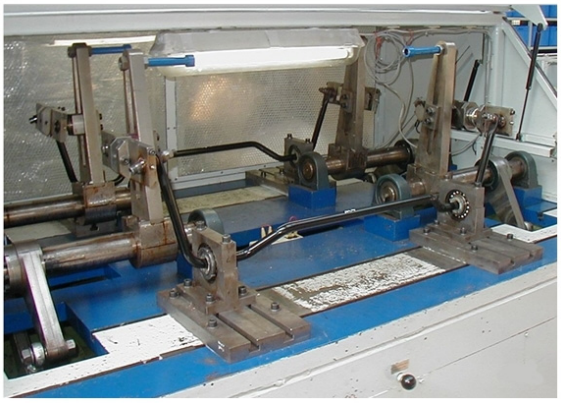

a

Eccentric type fatigue machine Franke 2 can simultaneously test two stabilizer bars

diameter of the stabilizer bar: 10 – 30mm
max. forces acting on the ends of the stabilizer bar: ± 6kN
oscillation angle: ± 20 °
frequenz: 1 – 6 Hz

b

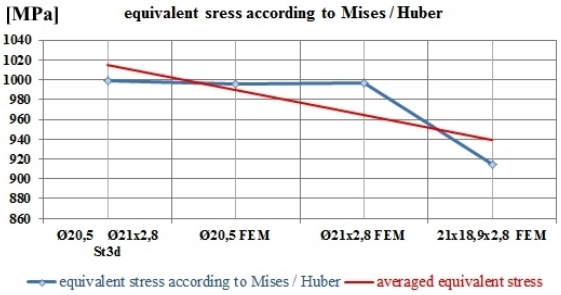

c

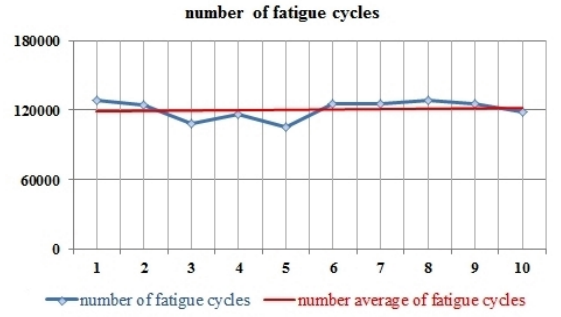

d

Fig. 11 The fatigue tests and their results (ThyssenKrupp Federn & Stabilisatoren GmbH): a) excentric type fatigue machine Franke 2, b) way mounting of stabilizer bar in the machine type Franke 2, c) equivalent stress according to Mises / Huber calculated using the analytical method and FEM for MQB stabilizer bar (with circular and elliptical cross–section), d) results of fatigue tests (number of fatigue cycles) carried out for the MQB stabilizer bar on the machine Franke 2

Since the stabilizer bar path (Tables 1 and 2) remains unchanged, the level of equivalent stresses is principally influenced by such parameters as: stabilizer bar geometry [4, 5], its cross–section in main radial areas and the required, assumed rigidity, thus the forces acting on the stabilizer bar ends. The stabilizer bars (MQB and Suzuki) were for fatigue tested (Fig. 11) and the results were compared with FEM calculations and simulations. Eccentric type fatigue machine Franke 2 was used, which can simultaneously test two stabilizer bars. The test parameters were the same as in FEM calculations. The results of tests and calculations are coincide (Fig.11 and Tables 1, 2).

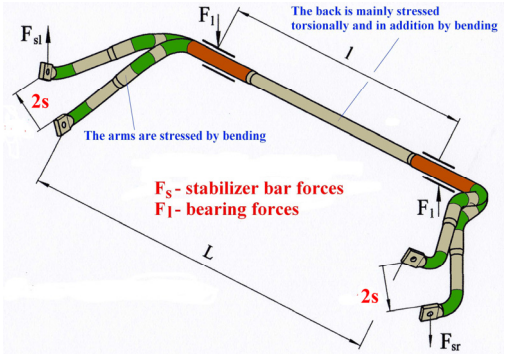

Fig. 12 Model of loaded stabilizer bar for FEM calculation

4. Conclusions

The change in cross–section does not automatically have to lead to increased equivalent stresses. The targeted and directed cross–section ovalization namely leads to the stress reduction (Figs. 5-10 and 11, c). Unfortunately, in reality the oval cross–sections do not remain constant. The changes take place as shown in Figs. 1 and 2. These changes in cross–section are difficult to consider in the analytical calculation process. The approximation of the cross–sections (item 2.1) should reduce the effort and the difficulty level. Unfortunately, in case of complex changes in cross–section also these calculations are too time-consuming and too complicated. Therefore the calculations with the FEM are used with increasing frequency.

As shown in the article, in the bending process, in which the ovalisation are directed and controlled, it can lead to positive results such as a decrease of the equivalent stress and exaltation of fatigue strength. Should not be forget, that the ovalisation can lead to microcracks and thus to premature failure of the stabilizer bars.

The design of devices for bending of stabilizer bars with the ability to control of ovalisation in radial zones of stabilizer bars is very complicated and requires a significant investment.

References

1. **Brendecke, T.; Götz, O.; Dziemballa, H.** 2009. Lightweight chassis through innovative materials and processes, in: Proc. ThyssenKrupp Technoforum: 69–73 (in German).
2. **Gebauer, H.P.** 2007. Stabilizer bars for motor vehicles / lecture, ThyssenKrupp Bilstein Suspension GmbH: 1–29 (in German).
3. **Heißing, B.; Ersoy, M.** 2008. Chassis handbook –

fundamentals, driving dynamics, components, systems, mechatronics, perspectives, second ed., Vieweg + Teubner, Wiesbaden (in German).
4. **Reimpell, J.; Betzler, J.W.** 2005. Chassis technology – fundamentals, fifth ed., Vogel Verlag, Würzburg (in German).
5. **Engel, B.** 2005. Bending of tubes, in: Proc., Fourth International Conf. Hydroumformung: 1–21 (in German).
6. **Kuczera, M.** 2009. Analysis of the Hamburg shaping of pipe bends, Dissertation, Akadamia Górniczo – Hutnicza im. S. Staszica, Kraków (in Polish).
7. **Śloderbach, Z.** 1998. Methods for calculating the output - the initial thickness of the pipe, which one is provided for bending, Przegląd Mechaniczny 2: 19 – 17 (in Polish).
8. **Litwin, P.; Stachowicz, F.** 2002. Elastic and bending moment in the pipe bending process. Experimental research and numerical simulation, Rudy i Metale Nieżelazne 47: 529-532.
9. **Stachowicz, F.** 2000. Bending with upsetting of copper tube elbows, Journal of Materials Processing Technology 100: 236-240. http://dx.doi.org/10.1016/S0924-0136(99)00478-1.
10. **Śloderbach, Z.** 2000. Analytical determination of the stored energy of plastic deformation during bending metal pipe benders, Przegląd Mechaniczny 9: 15-20 (in Polish).
11. **Damerow, T.** 2011. Investigation of the modification of geometry and related parameters of the semi-finished cross-section in bending of tubular stabilizer bars, Fachhochschule Südwestfalen, Diplomarbeit: 45-73 (in German).
12. **Abbott, P.** 2009. On the perimeter of an ellipse, The Mathematica Journal 11(2): 172-185. http://dx.doi.org/10.3888/tmj.11.2-4.
13. **Sykora, S.** 2005. Approximations of ellipse perimeters and of the complete elliptic integral E(x). Review of known formulae. Stan's Library, First ed..
14. **Abaqus Version 6.10**. 2010. Volume I: Static and dynamic analyses. Dessault Systems.
15. **Gebhardt, C.** 2011. FEM practice book with ANSYS Workbench. Introduction to linear and nonlinear mechanics, Carl Hanser Verlag, München: (in German).
16. **Klein, B.** 2007. FEM – Fundamentals and applications of finite element method in the machinery and transport equipment, seventh ed., Vieweg Studium Technik, Wiesbaden (in German).

A.M. Wittek, D. Gąska, B. Łazarz, T. Matyja

AUTOMOBILIŲ STABILIZATORIAI – STABILIZATORIŲ TRAUKIŲ STIPRUMO SKAIČIAVIMAI BEM, VAMZDINIŲ STABILIZATORIŲ APVALIŲJŲ DALIŲ OVALIZACIJA

R e z i u m ė

Ovalizacija ir mikro įtrūkimai gali ženkliai mažinti stabilizatoriaus traukės atsparumą nuovargiui ir to pasėkoje iššaukti jos pirmalaikį gedimą. Analitiniai stabilizatoriaus atsparumo skaičiavimai įvertinant ovalizaciją yra labai sudėtingi ir komplikuoti. Todėl vamzdinių stabilizatorių traukių atsparumas vis dažniau apskaičiuojamas BEM. Straipsnyje bendrais bruožais pateikiami vamzdinių stabilizatorių atsparumo skaičiavimai įvertinant vamzdžio deformacijas-ovalizaciją pagrindinėse apvalaus profilio srityse ir jo įtaką ekvivalentinio įtempimo reikšmei ir nuovargio atsparumui. Ištirti du plačiausiai naudojami automobilių stabilizatoriai įvertinant jų konstrukcinius ypatumus ir veikiančias apkrovas. Skaičiavimo rezultatai palyginti su ovalizacijos paveiktais stabilizatoriais (buvo išmatuoti stabilizatorių geometriniai parametrai ir tuo remiantis sukurti CAD ir baigtinių elementų modeliai). Be skaitinės analizės atlikti stabilizatorių nuovargio bandymai. Gauti rezultatai tarpusavyje palyginti. Atlikta vamzdinių stabilizatorių su ovalizuotu profiliu teorinė analizė.

A.M. Wittek, D. Gąska, B. Łazarz, T. Matyja

AUTOMOTIVE STABILIZER BARS – STABILIZER BAR STRENGTH CALCULATIONS USING FEM, OVALIZATION OF RADIAL AREAS OF TUBULAR STABILIZER BARS

S u m m a r y

The ovalization and microcracks may lead to a considerable reduction of the stabilizer bar fatigue strength and in consequence to its premature damage. Analytical stabilizer bar strength calculations taking the ovalization into consideration are very complex and complicated. Therefore, FEM is more and more frequently applied in tubular stabilizer bar strength calculations. The article presents an outline of tubular stabilizer bar strength calculations taking into consideration the tube deformation – ovalization in the main radial areas and its effect on the equivalent stress value and the fatigue strength. Two automotive stabilizer bars currently used in the industry with the assumption of actual constructional features and loads acting on it were analysed. The results were compared with the case of the occurrence of ovalization (geometric parameters of stabilizer bars were measured and on that basis the CAD and FEM models were made). In addition to numerical analysis, the results of fatigue tests performed on the selected stabilizer bar are presented and compared with the results of the numerical analysis. The whole article is complemented by theoretical analysis of the strength parameters of tubular stabilizer bar with shape ovalization.

Keywords: stabilizer bars, ovalization, fatigue, FEM method, simulation.

Received July 12, 2014
Accepted November 17, 2014